JOURNAL OF SOLID STATE CHEMISTRY 137, 82–86 (1998)
ARTICLE NO. SC977701

Relationship between Angles for Mn–O–Mn and Electrical Properties of Orthorhombic Perovskite-Type $(Ca_{1-x}Sr_x)MnO_3$

Hideki Taguchi,[1] Masanori Sonoda, and Mahiko Nagao

Research Laboratory for Surface Science, Faculty of Science, Okayama University, Okayama 700-8530, Japan

Received October 11, 1997; in revised form November 4, 1997; accepted November 10, 1997

Orthorhombic perovskite-type $(Ca_{1-x}Sr_x)MnO_3$ ($0 \le x \le 0.5$) was synthesized by a standard ceramic technique. The cell constants increase monotonously with increasing x. The Rietveld analysis indicates that the Mn–O(1 and 2) distances are independent of x, whereas the Mn–O(1 and 2)–Mn angles increase with increasing x. Measurements of the electrical resistivity (ρ) and the Seebeck coefficient (α) indicate that $(Ca_{1-x}Sr_x)MnO_3$ is an n-type semiconductor in the range $0 \le x \le 0.5$. Both the logarithm of the electrical resistivity ($\log \rho$) and the activation energy (E_a) increase while the mobility (μ) decreases with increasing x. From these results, it is considered that the Mn–O(1 and 2)–Mn angles play an important role in the electrical properties.

INTRODUCTION

$CaMnO_3$ has an orthorhombic perovskite-type structure and exhibits a weak ferromagnetism with $T_N = 123$ K (1). Poeppelmeier *et al.* prepared a single crystal of $CaMnO_3$ using a CaO–$CaCl_2$ flux and analyzed its structure by X-ray diffraction (2). The space group of $CaMnO_3$ is *Pnma* and the cell constants are $a = 0.5279$ nm, $b = 0.7448$ nm, and $c = 0.5264$ nm. $CaMnO_3$ is an n-type semiconductor and $\log \rho$ (ρ = electrical resistivity) vs $T^{-1/4}$ is linear at low temperature (3), which is indicative of variable-range hopping of electrons due to Anderson localization (4).

$SrMnO_3$ has a cubic perovskite-type structure with $a = 0.3802$ nm and is an insulator (5, 6). $SrMnO_3$ is an antiferromagnetic material with $T_N = 260$ K; a magnetic structure is expected from the superexchange interaction theory, which predicts antiferromagnetic Mn^{4+}–O^{2-}–Mn^{4+} interactions (7). Kafalas *et al.* measured the magnetic properties of the solid solution $(Ca_{1-x}Sr_x)MnO_3$, which is obtained by replacing some of the Ca^{2+} ions in $CaMnO_3$ with Sr^{2+} ions (8). With increasing Sr^{2+} content, T_N increases from ≈ 125 K ($x = 0$) to ≈ 175 K ($x = 0.5$), while the distortion and magnetic moment (σ) decrease. Takano *et al.* measured the magnetic hyperfine field of ^{119}Sn (Sn^{4+}) in $(Ca_{1-x}Sr_x)MnO_3$ by the Mössbauer effect (9). The magnetic hyperfine field for a Sn^{4+} ion depends linearly on the numbers of Ca^{2+} and Sr^{2+} ions in neighboring divalent cation sites. To explain these results, Takano *et al.* considered two kinds of spin transfer processes, contributing oppositely to the magnetic hyperfine field, and spin transfer through a divalent cation was particularly emphasized.

Although the electrical properties of $(Ca_{1-x}Sr_x)MnO_3$ are assumed to depend on the composition (x), there is no report on the electrical properties of $(Ca_{1-x}Sr_x)MnO_3$. In the present study, we synthesized orthorhombic perovskite-type $(Ca_{1-x}Sr_x)MnO_3$ ($0 \le x \le 0.5$) to study the relationship between the crystal structure and electrical properties. These results will provide information regarding the overlap between the manganese and oxygen orbitals in orthorhombic perovskite-type oxides.

EXPERIMENTAL

$(Ca_{1-x}Sr_x)MnO_3$ ($0 \le x \le 0.5$) was synthesized by a standard ceramic technique. $CaCO_3$, $SrCO_3$, and MnO_2 powders were weighted in appropriate proportions and milled with acetone. After the mixed powders were dried at 373 K, they were calcined at 1173 K for a few hours in air. The powders ($0 \le x \le 0.4$) were then fired at 1573 K for 24 hr under a flow of pure oxygen gas, while the powder ($x = 0.5$) was fired at 1573 K for 24 hr under a flow of pure argon gas. To measure the electrical resistivities, the samples were pressed into pellets under a pressure of 50 MPa. The pellets ($0 \le x \le 0.4$) were then sintered at 1573 K for 12 hr under a flow of pure oxygen gas, while the sample ($x = 0.5$) was sintered at 1573 K for 12 hr under a flow of pure argon gas. The samples obtained in this manner were further annealed at 973 K for 72 hr under a flow of pure oxygen gas.

The oxygen content in each sample was determined by the oxidation–reduction method (10). The crystal structure of the samples was identified by powder X-ray diffraction (XRD) with monochromatic Cu$K\alpha$ radiation. The structure refinement was carried out by Rietveld analysis with the

[1]To whom correspondence should be addressed.

0022-4596/98 $25.00

RIETAN program written by Izumi (11). XRD data were collected by step scanning over an angular range of $20^\circ \le 2\theta \le 100^\circ$ in increments of 0.02° (2θ) with monochromatic Cu$K\alpha$ radiation.

The electrical resistivity of the samples was measured by a standard four-electrode technique in the temperature range $40 \le T \le 973$ K. We attached platinum wires on the sintered samples with platinum paste as electrodes by annealing at 1173 K under a flow of pure oxygen gas. The Seebeck coefficient (α) was measured in the temperature range $300 \le T \le 525$ K, and the heating rate was 1 K/min.

RESULTS AND DISCUSSION

The powder XRD patterns of $(Ca_{1-x}Sr_x)MnO_3$ ($0 \le x \le 0.5$) annealed at 973 K under a flow of pure oxygen gas were completely indexed as the orthorhombic perovskite-type structure. The XRD pattern of the sample ($x = 0.5$) had both orthorhombic perovskite-type peaks and additional peaks of an unknown phase. The oxygen content of $(Ca_{1-x}Sr_x)MnO_3$ was determined to be 2.98–3.00 from chemical analysis.

The structure refinement of $(Ca_{1-x}Sr_x)MnO_3$ was carried out by Rietveld analysis of the XRD data. $CaMnO_3$ has the orthorhombic $GdFeO_3$-type structure with space group *Pnma* (2). In the present study, therefore, it can be concluded that $(Ca_{1-x}Sr_x)MnO_3$ has the same structure as $CaMnO_3$. Isotropic thermal parameters (B) for Ca, Sr, Mn, O(1), and O(2) ions were refined assuming that they had the same values. Refined structural parameters and residuals, R_{wp}, R_I, and R_F, are listed in Table 1. R_{wp}, R_I, and R_F are the weighted pattern, the integrated intensity, and the structure factor residuals, respectively.

TABLE 1
Refined Structure Parameters of $(Ca_{1-x}Sr_x)MnO_3$

Atom	Position	x	y	z	B
$x = 0$	$a = 0.52819(1)$ nm	$b = 0.74547(2)$ nm	$c = 0.52658(1)$ nm		
	$R_{wp} = 13.46\%$	$R_I = 4.68\%$	$R_F = 3.56\%$		
Ca	4(c)	0.034(1)	0.25	−0.005(3)	0.0018(10)
Mn	4(b)	0	0	0.5	0.0018(10)
O(1)	4(c)	0.491(3)	0.25	0.085(6)	0.0018(10)
O(2)	8(d)	0.287(3)	0.030(2)	−0.292(3)	0.0018(10)
$x = 0.2$	$a = 0.52962(2)$ nm	$b = 0.74970(3)$ nm	$c = 0.53011(2)$ nm		
	$R_{wp} = 12.77\%$	$R_I = 2.29\%$	$R_F = 2.88\%$		
Ca, Sr	4(c)	0.023(1)	0.25	−0.004(3)	0.0020(8)
Mn	4(b)	0	0	0.5	0.0020(8)
O(1)	4(c)	0.507(3)	0.25	0.067(7)	0.0020(8)
O(2)	8(d)	0.219(5)	0.025(3)	−0.215(5)	0.0020(8)
$x = 0.4$	$a = 0.53128(2)$ nm	$b = 0.75186(2)$ nm	$c = 0.53273(2)$ nm		
	$R_{wp} = 11.71\%$	$R_I = 2.64\%$	$R_F = 3.56\%$		
Ca, Sr	4(c)	0.0134(1)	0.25	−0.004(2)	0.0020(6)
Mn	4(b)	0	0	0.5	0.0020(6)
O(1)	4(c)	0.494(3)	0.25	0.045(7)	0.0020(6)
O(2)	8(d)	0.278(4)	0.027(3)	−0.273(4)	0.0020(6)
$x = 0.5$	$a = 0.53269(2)$ nm	$b = 0.75389(3)$ nm	$c = 0.53443(2)$ nm		
	$R_{wp} = 11.61\%$	$R_I = 2.61\%$	$R_F = 4.03\%$		
Ca, Sr	4(c)	0.008(1)	0.25	−0.001(3)	0.0023(6)
Mn	4(b)	0	0	0.5	0.0023(6)
O(1)	4(c)	0.491(5)	0.25	0.036(7)	0.0023(6)
O(2)	8(d)	0.279(4)	0.026(3)	−0.267(5)	0.0023(6)

Figure 1 shows the relationship between the cell constants (a-, b-, and c-axes) of $(Ca_{1-x}Sr_x)MnO_3$ and the composition (x). The cell constants increase monotonously with increasing x. The ionic radii of the Ca^{2+} and Sr^{2+} ions with a coordination number (CN) of 12 are 0.135 and 0.144 nm, respectively (12). Therefore, it is obvious that an increase in the cell constants corresponds to the difference in the ionic radii between the Ca^{2+} and Sr^{2+} ions. In orthorhombic perovskite-type $(Ca_{1-x}Sr_x)MnO_3$, A-site cations (Ca and Sr ions) coordinate with 12 anions: 4 O(1) and 8 O(2) ions. B-site cations (Mn ions) coordinate with 6 anions: 2 O(1) and 4 O(2) ions. Table 2 shows the Mn–O(1 and 2) distances and the Mn–O(1 and 2)–Mn angles calculated from the refined structural parameters. Although the cell constants increase with increasing x, the Mn–O(1 and 2) distances are nearly independent of x or decrease little. The O(1)–Mn–O(1), O(1)–Mn–O(2), and O(2)–Mn–O(2) angles are 180°, 90°, and 90° or 180°, respectively. The Mn–O(1 and 2)–Mn angles are less than 180° and increase with increasing x.

Figure 2 shows the relationship between the logarithm of the electrical resistivity ($\log \rho$) of $(Ca_{1-x}Sr_x)MnO_3$ and the reciprocal temperature ($1000/T$). Kafalas *et al.* reported that $(Ca_{1-x}Sr_x)MnO_3$ ($0 \le x \le 0.5$) exhibits weak ferromagnetism and T_N increases linearly with increasing x (8). Using their results, we estimated T_N for $x = 0.2$ and 0.4. T_N for $(Ca_{1-x}Sr_x)MnO_3$ is indicated by the arrows in Fig. 2. The $\log \rho$–$1000/T$ curve for $CaMnO_3$ ($x = 0$) is not linear. At low temperature, $\log \rho$ increases with increasing x. Above ≈ 135 K, however, $\log \rho$ for $x = 0$ is larger than $\log \rho$ for $x = 0.2$. The $\log \rho$–$1000/T$ curves are linear above T_N: $140 \le T \le 650$ K for $x = 0.2$, $170 \le T \le 375$ K for $x = 0.4$, and $190 \le T \le 575$ K for $x = 0.4$. The nonlinear $\log \rho$–$1000/T$ curve for $CaMnO_3$ ($x = 0$) is explained by the variable-range hopping of electrons due to Anderson localization (3, 4). The electrical conductivity (σ) for $CaMnO_3$ ($x = 0$) is given by

$$\sigma = A \exp\{-(Q/kT)^{1/4}\}, \quad [1]$$

where A is a constant depending on the assumption made about the electron–phonon interaction and k is the Boltzmann constant. Q is a constant given by

$$Q \propto 1/\alpha^3 N(E), \quad [2]$$

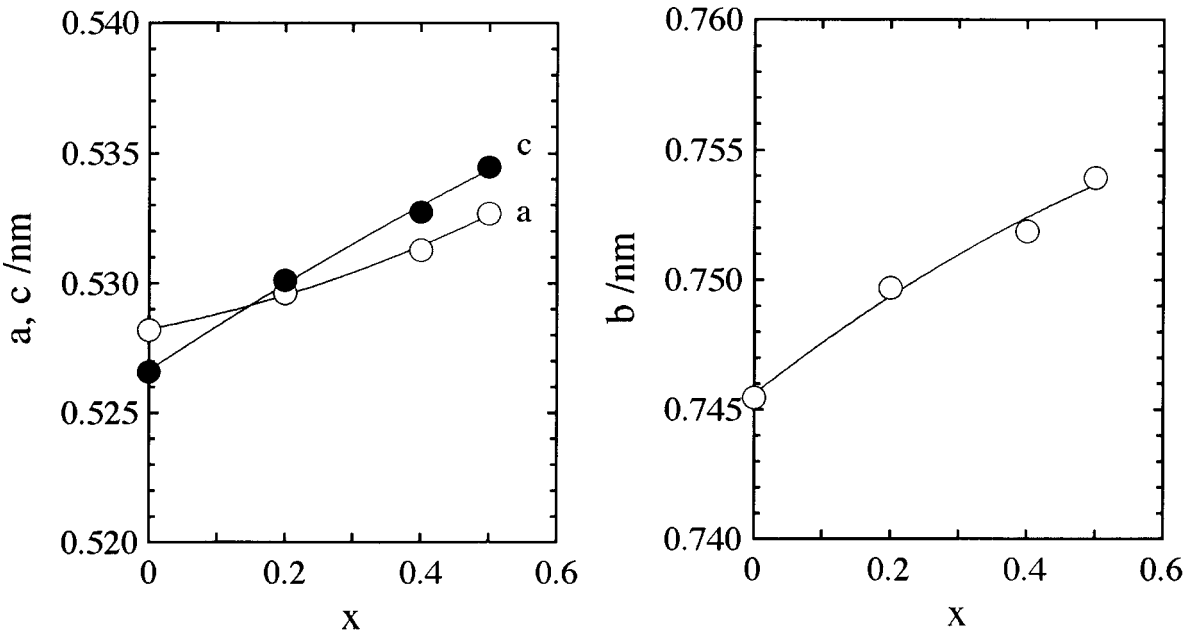

FIG. 1. Cell constants (*a*-, *b*-, and *c*-axes) vs composition (x) for the system $(Ca_{1-x}Sr_x)MnO_3$.

where α denotes the rate of fall-off of the envelope of the wave function and $N(E)$ is the density of states at the Fermi level (13). The electrical conductivity (σ) for $(Ca_{1-x}Sr_x)MnO_3$ ($0.2 \leq x \leq 0.5$) is given by

$$\sigma = \sigma_0 \exp(-E_a/kT), \qquad [3]$$

where σ_0 is the specific electrical conductivity at $T = 0$ K and E_a is the activation energy that is calculated from the linear part of the log ρ–$1000/T$ curve.

Figure 3 shows the relationship between the Seebeck coefficient (α) of $(Ca_{1-x}Sr_x)MnO_3$ and temperature, α at $\approx$330 K is -0.068 mV/K ($x = 0$), -0.104 mV/K ($x = 0.2$), -0.110 mV/K ($x = 0.4$), and -0.121 mV/K ($x = 0.5$). This result indicates that $(Ca_{1-x}Sr_x)MnO_3$ ($0 \leq x \leq 0.5$) is an n-type semiconductor. α of $CaMnO_3$ ($x = 0$) decreases gradually with increasing temperature, whereas α of $(Ca_{1-x}Sr_x)MnO_3$ ($0.2 \leq x \leq 0.5$) is independent of temperature. The variation of α suggests that the electrical conductivity of $CaMnO_3$ ($x = 0$) is slightly different from the electrical conductivity of $(Ca_{1-x}Sr_x)MnO_3$ ($0.2 \leq x \leq 0.5$). To explain the temperature independence of α, Tuller and Nowick proposed an equation for a hopping mechanism involving a fixed number of carriers (14). Under the assumption that all other interaction effects are negligible, the following equation is obtained:

$$\alpha = \pm \frac{k}{e}\left\{\ln \beta\left(\frac{1-c}{c}\right) + \frac{S_T^*}{k}\right\}. \qquad [4]$$

Here S_T^* is the vibration entropy and usually can be neglected. β is a degeneracy factor; for the case of $\beta = 1$, Eq. [4] is often referred to as the Heikes formula (14). c. is the fraction of sites which contain the electron.

$$c = \frac{n}{N}, \qquad [5]$$

where n is the number of carriers and N is the number of available sites per unit volume (V). V is easily calculated from the cell constants. Since there are four sites in the orthorhombic perovskite-type unit cell, N is expressed as $N = 4/V$. By substituting Eq. [5] into Eq. [4], n is obtained

$$n = \frac{4}{V}\left\{\frac{1}{\exp(\pm \alpha e/k) + 1}\right\} \qquad [6]$$

TABLE 2
Mn–O(1 and 2) Distances (nm) and Mn–O(1 and 2)–Mn Angles (deg) of $(Ca_{1-x}Sr_x)MnO_3$

	$x = 0$	$x = 0.2$	$x = 0.4$	$x = 0.5$
Mn–O(1) × 2	0.192(1)	0.191(1)	0.190(1)	0.189(1)
Mn–O(2) × 2	0.188(2)	0.189(4)	0.189(3)	0.186(3)
Mn–O(2) × 2	0.192(2)	0.191(4)	0.192(3)	0.195(3)
Mn–O(1)–Mn	152.8(18)	156.7(18)	165.2(22)	168.1(22)
Mn–O(2)–Mn	157.5(09)	161.8(10)	163.1(11)	164.3(11)

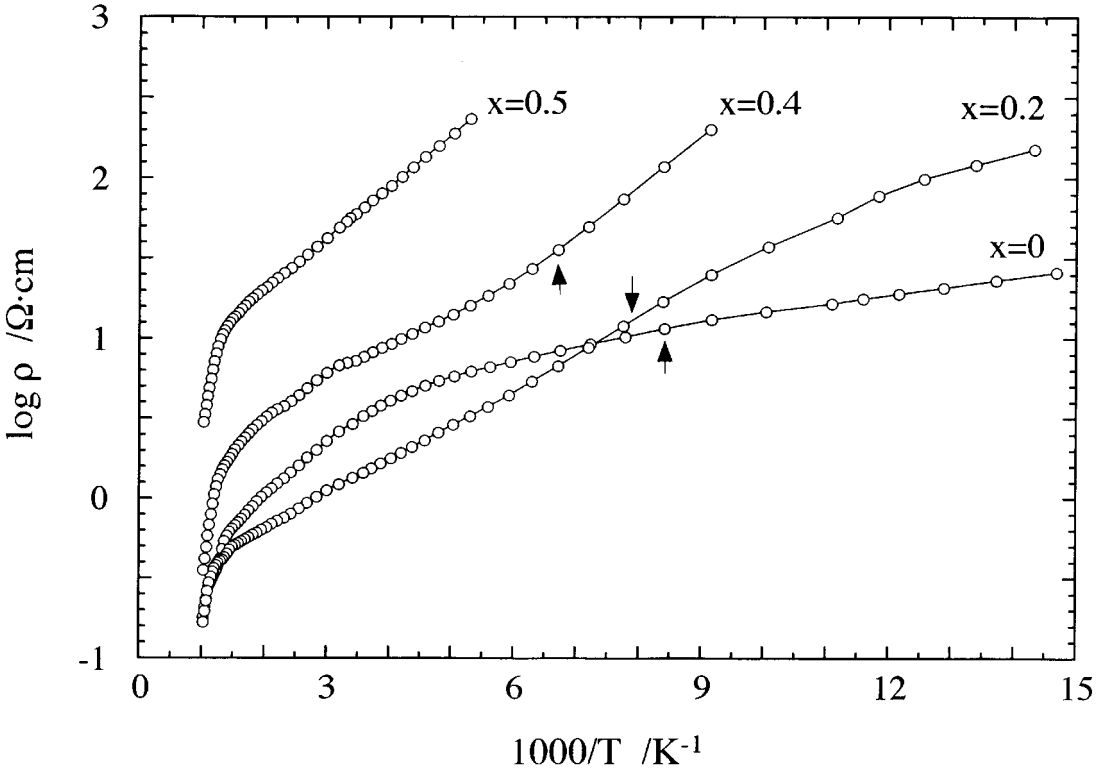

FIG. 2. Logarithm of the electrical resistivity (log ρ) vs reciprocal temperature ($1000/T$) for the system $(Ca_{1-x}Sr_x)MnO_3$. The arrows indicate the Néel temperature (T_N).

and is calculated from α and N. The mobility (μ) is given by

$$\mu = \frac{\sigma}{en}, \qquad [7]$$

where σ is the electrical conductivity. For $(Ca_{1-x}Sr_x)MnO_3$ ($0.2 \le x \le 0.5$) at ≈ 330 K, n is $\approx 1.9 \times 10^{22}$ and independent of x, whereas μ decreases with increasing x: $\approx 2.9 \times 10^{-4}\ cm^2 \cdot V^{-1} \cdot s^{-1}$ ($x = 0.2$), $\approx 5.5 \times 10^{-5}\ cm^2 \cdot V^{-1} \cdot s^{-1}$ ($x = 0.4$), and $\approx 7.9 \times 10^{-6}\ cm^2 \cdot V^{-1} \cdot s^{-1}$ ($x = 0.5$).

The MnO_6 octahedron in $(Ca_{1-x}Sr_x)MnO_3$ connects at O(1) or O(2) of another MnO_6 octahedron. There are two kinds of cation–anion–cation overlap; one is an overlap (π-bonding) between the cation $d\varepsilon$ and oxygen p_π orbitals, and the other is the overlap (σ-bonding) between the cation $d\gamma$ and oxygen p_σ orbitals (15). Since $(Ca_{1-x}Sr_x)MnO_3$ ($0 \le x \le 0.5$) has no oxygen deficiency from the chemical analysis, the valence of the Mn ion is $4+$. The Mn^{4+} ion has the electron configuration with $(d\varepsilon)^3(d\gamma)^0$. In $(Ca_{1-x}Sr_x)MnO_3$ ($0 \le x \le 0.5$), therefore, it is not necessary to consider the overlap (σ-bonding) between the cation $d\gamma$ and oxygen p_σ orbitals. The linear relationship of the log ρ–$10/T^{1/4}$ curve indicates that the electrical conductivity of $CaMnO_3$ ($x = 0$) can be related to variable-range hopping of electrons due to Anderson localization. On the other hand, the linear relationship of the log ρ–$1000/T$ curve of $(Ca_{1-x}Sr_x)MnO_3$ ($0.2 \le x \le 0.5$) indicates that three $3d$ electrons of the Mn^{4+} ion are localized and the Fermi level lies between the $d\varepsilon$* levels and the $d\gamma$* levels. Both the $d\varepsilon$* and $d\gamma$* levels are localized and narrow, and the cation–anion–cation overlap integrals (Δ^{π}_{cac} for π-bonding and Δ^{σ}_{cac} for σ-bonding) are smaller than the critical overlap integral (Δ_c); $\Delta^{\pi}_{cac} < \Delta^{\sigma}_{cac} < \Delta_c$ (15). Although the Mn–O(1 and 2) distances are independent of x, the Mn–O(1 and 2)–Mn angles increase with increasing x. It is considered that the increase in the Mn–O(1 and 2)–Mn angles makes the π-bonding decrease. Therefore, log ρ and E_a increase while μ decreases with increasing x. From these results, it is considered that the Mn–O(1 and 2)–Mn angles play an important role in the electrical properties of $(Ca_{1-x}Sr_x)MnO_3$.

CONCLUSION

Orthorhombic perovskite-type $(Ca_{1-x}Sr_x)MnO_3$ was synthesized in the range $0 \le x \le 0.5$. From Rietveld analysis, it follows that the Mn–O(1 and 2) distances are independent of x, whereas the Mn–O(1 and 2)–Mn angles increase with increasing x. Measurements of the electrical resistivity and the Seebeck coefficient indicate that $(Ca_{1-x}Sr_x)MnO_3$

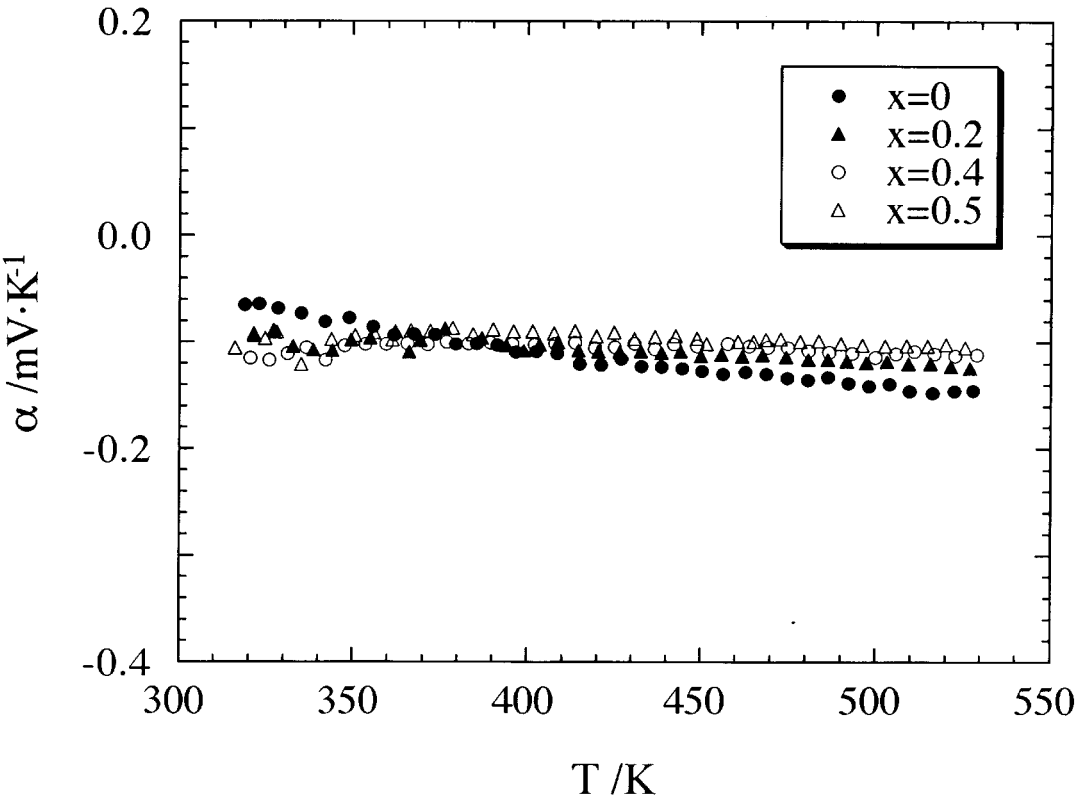

FIG. 3. Seebeck coefficient (α) vs temperature (T) for the system $(Ca_{1-x}Sr_x)MnO_3$.

is an n-type semiconductor in the range $0 \leq x \leq 0.5$. Both $\log \rho$ and E_a increase while μ decreases with increasing x. From these results, it is considered that the increase in the Mn–O(1 and 2)–Mn angles makes the π-bonding decrease.

ACKNOWLEDGMENT

This work was partly supported by a Grant-in-Aid for Scientific Research (Priority Area 274, Grant No. 09229240) from the Ministry of Education, Science, and Culture of Japan.

REFERENCES

1. J. B. MacCesney, H. J. William, J. F. Potter, and R. C. Sherwood, *Phys. Rev.* **164,** 779 (1967).
2. K. R. Poeppelmeier, M. E. Leonowicz, J. C. Scanlon, and W. B. Yelon, *J. Solid State Chem.* **45,** 71 (1982).
3. H. Taguchi, *Phys. Status Solidi A* **88,** K79 (1985).
4. N. F. Mott, *Adv. Phys.* **21,** 785 (1972).
5. T. Negas and R. Roth, *J. Solid State Chem.* **1,** 409 (1970).
6. K. Kamata and T. Nakamura, *J. Phys. Soc. Jpn.* **35,** 1558 (1973).
7. T. Takeda and S. Ohara, *J. Phys. Soc. Jpn.* **37,** 275 (1974).
8. J. A. Kafalas, N. Menyuk, K. Dwight, and J. M. Longo, *J. Appl. Phys.* **42,** 1497 (1971).
9. M. Takano, Y. Takeda, M. Shimada, T. Matsuzawa, and T. Shinjyo, *J. Phys. Soc. Jpn.* **39,** 656 (1975).
10. H. Taguchi, H. Yoshioka, D. Matsuda, and M. Nagao, *J. Solid State Chem.* **104,** 460 (1993).
11. F. Izumi, "The Rietveld Method," p. 236. Oxford University Press, Oxford, 1993.
12. R. D. Shannon and C. T. Prewitt, *Acta Crystallogr., Sect. B* **25**, 925 (1969).
13. N. Mott, "Metal–Insulator Transition," p. 35. Taylor & Francis Ltd., London, 1974.
14. H. L. Tuller and A. S. Nowick, *J. Phys. Chem. Solids* **38,** 859 (1977).
15. J. B. Goodenough, *Czech. J. Phys. Sect. B* **17,** 304 (1967).